



# Molecular dynamics simulations of negatively charged DPPC/DPPI lipid bilayers at two levels of resolution



T.B. Stanishneva-Konovalova, O.S. Sokolova\*

M.V. Lomonosov Moscow State University, 1 Leninskie Gory, Bld. 12, Moscow 119991, Russia

## ARTICLE INFO

### Article history:

Received 7 January 2014  
Received in revised form 24 April 2014  
Accepted 30 April 2014  
Available online 9 May 2014

### Keywords:

Molecular dynamics  
Coarse-grained  
DPPC  
PI(4,5)P<sub>2</sub>

## ABSTRACT

Lipid membranes are highly dynamic structures involved in various cell biological processes which are regulated by a large number of proteins. Computer simulations can provide a dynamic picture with atomistic details of membrane behavior and its interactions with macromolecules. Here we use molecular modeling at two levels of resolution, united-atom and coarse-grained, to investigate the lipid–lipid interactions within the model bilayers composed of charged PI(4,5)P<sub>2</sub> and neutral DPPC lipids. The united-atom representation allows us to simulate two lipid bilayers containing different numbers of charged lipid molecules. To characterize these systems we compared the area and volume per lipid, bilayer thickness, deuterium order parameter and lateral diffusion coefficients. The united-atom results indicate that the increase of PI(4,5)P<sub>2</sub> lipids in the membrane leads to the higher ordering of neutral lipids. Bilayer properties calculated from the coarse-grained simulation were in good agreement with the united-atom results.

© 2014 Elsevier B.V. All rights reserved.

## 1. Introduction

Lipid membranes are highly dynamic structures involved in various cell biological processes such as morphogenesis, endo- and phagocytosis, cell motility, vesicular transport [1,2]. These processes are regulated by a large number of proteins including a group of proteins directly binding to membranes and modulating their shape [3–5]. Many of these proteins have varied binding affinities for charged phospholipids, particularly phosphoinositides [6–9]. Phosphoinositides (PIPs) are phosphorylated derivatives of phosphatidylinositol, a lipid molecule found in the cytosolic leaflet of the cell plasma membrane and in membranes of several intracellular organelles [10]. Depending on the cell type, PIPs constitute ~1–2% of the total phospholipids in the plasma membrane. PIPs are known to spatially aggregate into PIP-enriched rafts, and thus raise their local concentration [11,12]. Phosphatidylinositol 4,5-bisphosphate (PI(4,5)P<sub>2</sub>) is the most abundant phosphoinositide acting as an ubiquitous second messenger and as a precursor

to other second messengers, such as diacylglycerol (DAG), D-myoinositol 1,4,5-trisphosphate (IP<sub>3</sub>), and phosphatidylinositol 3,4,5-trisphosphate (PIP<sub>3</sub>) [13–15]. The fatty acids of PIP<sub>2</sub> are variable in different species and tissues but in mammals the most common fatty acids are stearic in position 1 and arachidonic in position 2 [16].

A combination of biochemical, diffraction and spectroscopic techniques is used to study PIPs synthesis, aggregation and cell localization. Computer simulations can provide a dynamic picture with atomistic details of PIP-containing membrane behavior and its interactions with macromolecules. Several studies have used MD simulations to explore the interactions of PIP<sub>2</sub> with specific residues of peptides and proteins [17–21]. Another study investigates the interaction of PIP<sub>2</sub> with neighboring lipids and its organization within the lipid bilayer [22]. It suggests that PIP<sub>2</sub> reorganizes the neighboring lipids and induces the formation of a PIP<sub>2</sub> lipid microdomain which allows it to act as a protein-anchoring molecule.

Many modifications of the classical MD method have been developed recently and one of them is the coarse-grained (CG) method [23]. In CG models molecules are described by the interaction sites representing groups of atoms, providing a reduced resolution description of the given system. It allows one to simulate large systems on time scales inaccessible to simulations with an explicit all-atom and a united-atom representations.

*Abbreviations:* CG, coarse-grained; DMPC, dimyristoylphosphatidylcholine; DMPG, dimyristoylphosphatidylglycerol; DPPC, dipalmitoylphosphatidylcholine; DPPI, dipalmitoylphosphatidylinositol 4,5-bisphosphate; PI(4,5)P<sub>2</sub>, phosphatidylinositol 4,5-bisphosphate; PIP, phosphoinositide; POPC, palmitoyl-oleoyl phosphatidylcholine; POPS, palmitoyl-oleoyl phosphatidylserine.

\* Corresponding author. Tel.: +7 495 9380005; fax: +7 495 9395738.

E-mail address: [sokolova184@gmail.com](mailto:sokolova184@gmail.com) (O.S. Sokolova).

In the present study we investigated lipid bilayers composed of dipalmitoylphosphatidylcholine (DPPC) and dipalmitoylphosphatidylinositol 4,5-bisphosphate (DPPI) at two levels of resolution: united-atom and coarse-grained. Using the united-atom representation we simulated two lipid bilayers: 127 DPPC/1 DPPI and 116 DPPC/12 DPPI. To characterize our systems we compared several parameters: the area and volume per lipid, bilayer thickness, deuterium order parameter and lateral diffusion coefficient.

## 2. Methods

All simulations were carried out in GROMACS 4.5.3 [24].

### 2.1. United-atom simulations

Using a united-atom representation we studied two systems: (1) a bilayer composed of 127 DPPC and 1 DPPI; (2) a bilayer composed of 116 DPPC and 12 DPPI. The first structure was taken from Holdbrook [25]. The number of DPPI lipids was then increased to six in each leaflet by changing 11 phosphatidylcholine headgroups to phosphatidylinositol 4,5-bisphosphate in the PyMOL program (<http://www.pymol.org/>). Topology for the DPPC lipid corresponds to the DPPC3 topology in Kukul [26]. That is the original DPPC topology included in the Gromos53a6 force field distribution with the following alterations: partial charges of the lipid headgroup were modified as in Chandrasekhar et al. [27] (model C) and the ester-carbonyl carbon atom type was changed from “C” to “CH0” as suggested in the same publication. The DPPI topology was taken from Holdbrook [25]. The initial size of both systems was  $5.55 \times 6.89 \times 7.08$  nm. SPC water model was used as a solvent to which 100 mM of NaCl were added to reproduce the physiological salt concentration. Since DPPI lipids carry a negative charge, additional ions of Na were added to neutralize the system.

Prior to simulations both systems were minimized using the steepest descent method for 1000 steps. The simulation parameters for both simulations were as recommended in Piggot et al. [28] for the Gromos53a6 force field. The Coulomb interactions were truncated at 0.9 nm. The van der Waals interactions were treated using a twin-range cutoff with the short-range interactions truncated at 0.9 nm and the long-range interactions at 1.4 nm. The long range electrostatic interactions were treated with the PME method [29] using a grid spacing of 0.12 nm with a cubic interpolation. A long-range dispersion correction was applied to the energy and pressure. The pressure was maintained at 1 bar using the Parrinello-Rahman algorithm [30,31] with a time constant of 5 ps applied semiisotropically. Nose-Hoover thermostat [32,33] with a time constant of 0.5 ps was used to maintain temperature at 323 K. Both systems were simulated for 150 ns with a time step 2 fs.

To analyze the impact of DPPI lipids on DPPC bilayer properties we compared several parameters: the area per lipid, volume per lipid, bilayer thickness, deuterium order parameters and lateral diffusion coefficients. All the parameters were averaged throughout the trajectory and compared with experimental data for pure DPPC lipid bilayers.

The average area per lipid was calculated by dividing the box area in the dimension parallel to the plane of the bilayer by the number of lipids in each leaflet.

The volume per lipid was determined as  $V_L = (V_B - V_W)/2n_L$ , where  $V_B$  is the simulation box volume,  $V_W$  is the volume of a box with the same number of water molecules at the same conditions as the target system and  $n_L$  is the number of lipids in each leaflet.

The bilayer thickness was calculated as the distance between the peaks of the lipid headgroup electron density, namely the

choline group. The electron density profiles were determined using the *g\_density* program from the GROMACS package.

The deuterium order parameter is defined as:

$$S_{CD} = 1/2(3 \cos^2 \theta - 1),$$

where  $\theta$  is the angle between the carbon–deuterium bond and the bilayer normal, brackets denote the averaging over the time and over all phospholipids.  $S_{CD}$  was calculated in GROMACS by using *g\_order* which allows to calculate  $S_{CD}$  without the need of explicit hydrogens.

The lateral diffusion coefficient for DPPC lipids was calculated from the Einstein relation for the mean square displacement:  $MSD = 4D_{lat}t$  for long times  $t$ . It was calculated on the linear zone of the MSD curve and averaged over all DPPC lipids. Calculations of MSD were performed with *g\_msd* program of GROMACS.

### 2.2. Coarse-grained simulations

After 150 ns of simulation, the bilayer composed of 116 DPPC and 12 DPPI was converted from the united-atom into the coarse-grained representation using the *g\_fg2cg* program of GROMACS 4.5.3. The correlation between united atoms and coarse-grained atoms is provided in the mapping section of a lipid topology. The mapping scheme for DPPC was proposed by Marrink et al. [34]. The DPPI mapping scheme in this work was based on materials from Lopez et al. [35] and Levtsova [36] (Fig. 1A). After the conversion the coarse-grained bilayer patch was replicated five times over the X-axis and then two times over the Y-axis. Thus we created a ten times larger bilayer composed of 1160 DPPC and 120 DPPI (Fig. 1B). Polarizable water molecules and ions were added to the system.

For coarse-grained dynamics the Martini force field was used [23]. The parameters were as recommended at Marini's official website for simulations with the polarizable water model (<http://md.chem.rug.nl/cgmartini/>) [37]. Standard cut-off schemes are used for the non-bonded interactions in the Martini model: LJ interactions are shifted to zero in the range 0.9–1.2 nm, and electrostatic interactions in the range 0.0–1.2 nm. Long range electrostatics are treated with the PME algorithm. As for the united-atom simulations, the Parrinello-Rahman algorithm with a time constant of 5 ps applied semiisotropically was used to maintain the pressure at 1 bar. Nose-Hoover thermostat with a time constant of 2 ps was used to maintain temperature at 323 K.

In the Martini force field all atom masses are set to 72 amu for reasons of computational efficiency which may affect the system behavior. We performed two simulation runs for the same coarse-grained lipid bilayer: first with masses by default and second with masses corresponding to united-atom representation. The systems were simulated for 70 and 100 ns respectively with the time step of 20 fs. To characterize the coarse-grained bilayers we analyzed the same set of parameters as for the united-atom simulations except for the deuterium order parameter which requires an explicit lipid chain representation.

The reported study was performed at the Supercomputing Center of Lomonosov Moscow State University [38].

## 3. Results and discussion

### 3.1. United-atom simulations

In the present study we investigated dipalmitoylphosphatidylcholine (DPPC)/dipalmitoylphosphatidylinositol 4,5-bisphosphate (DPPI) lipid bilayers in two levels of resolution: united-atom and coarse-grained. Using the united-atom representation we simulated

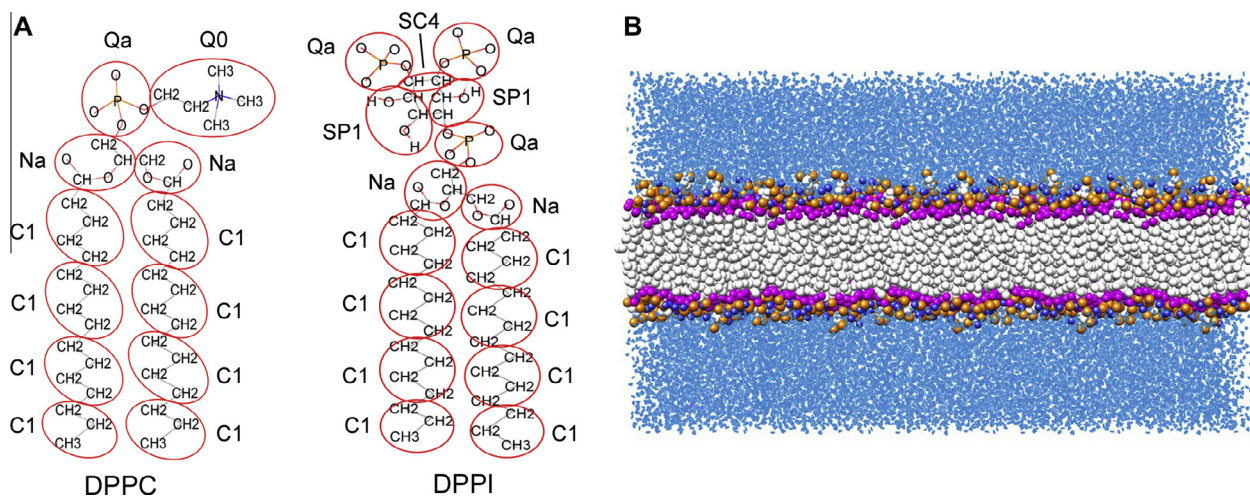


**Fig. 1.** Coarse-grained simulations. (A) Mapping schemes for DPPC and DPPI lipids. Red circles show atoms united in one coarse-grained atom in the Martini force field. (B) Coarse-grained model of 1160 DPPC/120 DPPI lipid bilayer in water. (For interpretation of the references to color in this figure legend, the reader is referred to the web version of this article.)

a lipid bilayer with less than 1% DPPI and a bilayer with 9% DPPI and compared their properties.

For the bilayer containing 127 DPPC and 1 DPPI the area per lipid averaged on the interval 100–150 ns was  $0.57 \text{ nm}^2$  which is lower than experimentally obtained values for pure DPPC bilayers ( $0.63\text{--}0.64 \text{ nm}^2$ ) [39–43]. The bilayer containing 12 DPPI demonstrates further decrease of the a.p.l. to  $0.53 \text{ nm}^2$  (Fig. 2A). The volume per lipid was 1.21 and  $1.14 \text{ nm}^3$  for the 1st and the 2nd bilayers respectively, while the experimental data show  $1.23 \text{ nm}^3$  [42,43]. The bilayer thickness, on the contrary, was lower for the bilayer with one DPPI lipid: 4.2 opposed to 4.5 nm. Both values were higher than experimentally obtained 3.8 nm [39–43]. The described changes in bilayer properties may be caused by the straightening of lipid acyl chains and the process of lipid ordering. To prove this hypothesis we calculated deuterium order parameters for both acyl chains of DPPC lipids and compared it to experimental data for the 1st chain (Fig. 2C and D) [44]. Values were higher in the system with 12 DPPI lipids and both curves lied above the experimental curve which indicates increase in lipid ordering. The lateral diffusion coefficient for DPPC lipids was calculated on the linear interval of the MSD curves from 30 to 110 ns:  $1.33 \times 10^{-7}$  and  $1.02 \times 10^{-7} \text{ cm}^2/\text{s}$  for bilayers with 1 DPPI and 12 DPPI respectively (Fig. 2B). Experimentally obtained values for 321 K are  $0.85\text{--}1.2 \times 10^{-7} \text{ cm}^2/\text{s}$  [45].

All these data indicate that the increase of DPPI lipid amount leads to the increase of the order of DPPC lipids. For the system containing only one DPPI molecule all of the examined parameters were close to the experimentally obtained values for pure DPPC membranes. However, lower values of the area per lipid, higher values of the bilayer thickness and especially the deuterium order parameter imply a certain difference in DPPC lipid organization. This difference becomes more significant when the number of DPPI lipid is raised to six in each leaflet.

### 3.2. Coarse-grained simulations

Next, we carried on the investigation of a larger lipid bilayer, also containing 9% of PIP<sub>2</sub>. For this purpose the coarse-grained method was used because it requires less computational resources allowing us to reach larger system sizes and time scales.

The united-atom bilayer composed of 116 DPPC and 12 DPPI was used to create a coarse-grained bilayer patch of 1160 DPPC and 120 DPPI. We performed two 70 ns simulation runs for this

bilayer: with atom masses by default (all equal to 72 amu in the Martini force field) and with masses corresponding to the united-atom representation. To evaluate the quality of our coarse-grained model we compared its parameters with the values calculated from the united-atom simulation.

Changing masses of coarse-grained atoms from the default to more appropriate values had no significant effect on bilayer properties (see comparison of a.p.l. on Fig. 3) but required much more computer resources. Thus we only used masses by default in coarse-grained simulations later on and extended the simulation run to 100 ns. Parameters for the coarse-grain system are shown in Table 1.

The increase of the area per lipid and decrease of the bilayer thickness indicate that the coarse-grained simulations provide a more disordered representation of DPPC lipids. The effect of DPPI presence thus may be imperceptible if values calculated from a coarse-grained simulation are compared to experimental values for pure DPPC bilayer. To capture this effect the comparison should be made between coarse-grained models of pure DPPC bilayer and DPPC/DPPI bilayer. A more noticeable difference was observed in diffusion coefficients (Table 1). As it was described by Marrink [23], the dynamics observed with CG models is 2- to 10-times faster in comparison to atomistic models. The main reason is the absence of friction arising from the atomic degrees of freedom which are missing in CG models. The effective time sampling may be found on the basis of comparison of diffusion constants in CG and atomistically modeled systems. For the interpretation of the CG simulation results one can simply scale the time axis to a first approximation. This approximation describes the general dynamics of various systems quite well. For example, water permeation rates across a DPPC membrane [34] and aggregation of lipids into vesicles [46] are in good agreement with experimental measurements after scaling the rates by a factor of four. In case of our DPPC/DPPI bilayers the conversion factor is 2.5.

Above we compared two united-atom models: 127 DPPC/1 DPPI and 116 DPPC/12 DPPI. We demonstrated that the increase of amount of DPPI leads to the reduction of area per lipid, volume per lipid and DPPC lateral diffusion coefficient. In contrast, the bilayer thickness and deuterium order parameter show higher values. All these data indicate that the DPPI lipid orders the DPPC lipids around it. Our results are in agreement with MD simulation experiments performed earlier for a single PIP<sub>2</sub> lipid molecule, incorporated into a model lipid bilayer that contains 71 DPPC [22].

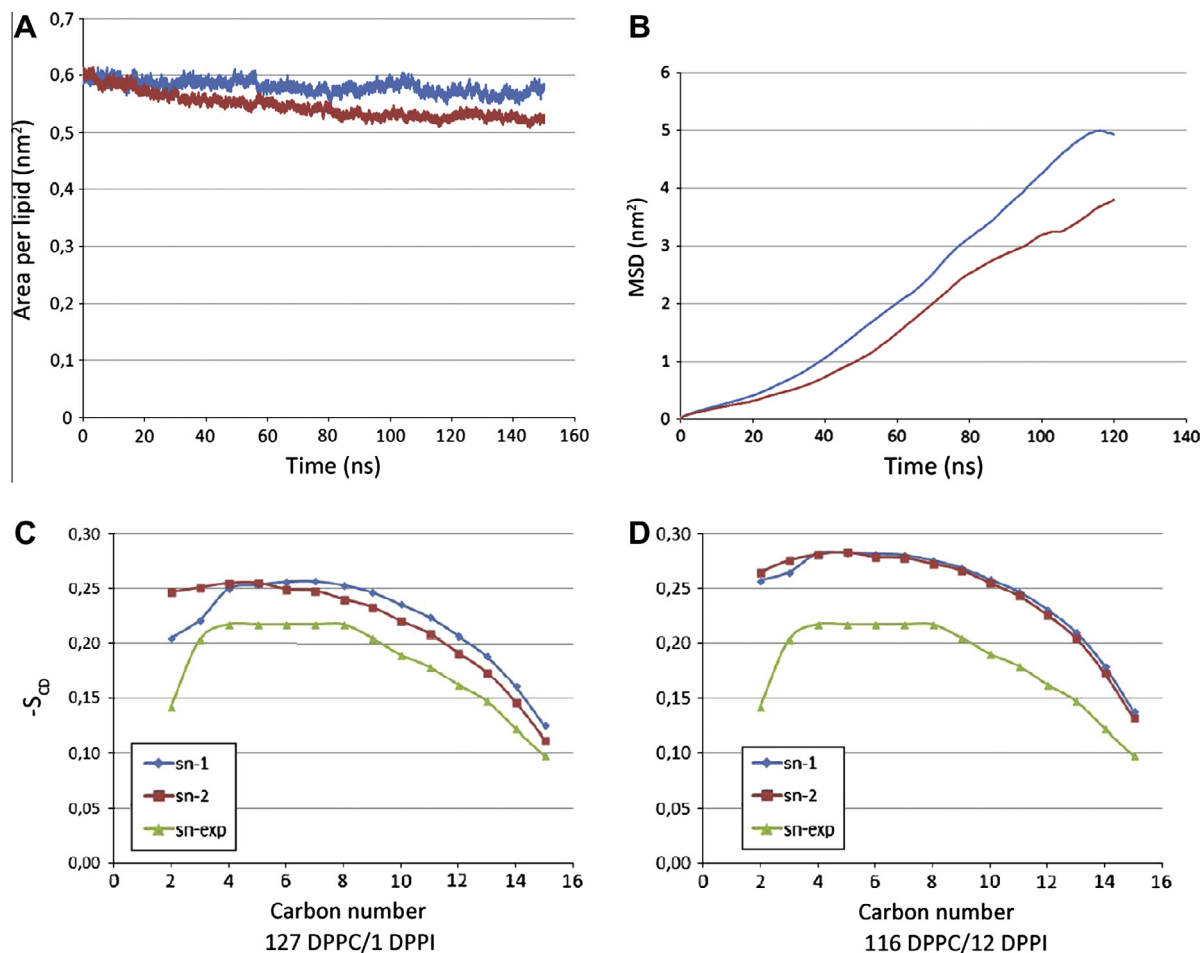


**Fig. 2.** United-atom simulations. (A) Area per lipid for the 127 DPPC/1 DPPI bilayer (blue curve) and the 116 DPPC/12 DPPI bilayer (red curve). (B) Mean square displacement (MSD) of DPPC lipids in the 127 DPPC/1 DPPI bilayer (blue curve) and the 116 DPPC/12 DPPI bilayer (red curve). The coefficient was calculated over the linear interval from 30 to 110 ns. (C) Deuterium order parameters for acid chains of DPPC lipids for systems, containing 1 DPPI and (D) 12 DPPI. Blue and red curves correspond to united-atom simulation results, green curve corresponds to experimental data. (For interpretation of the references to color in this figure legend, the reader is referred to the web version of this article.)

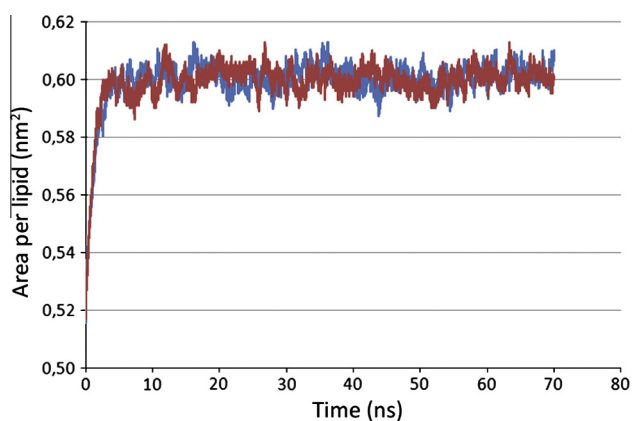


**Fig. 3.** Area per lipid for coarse-grained simulations with masses by default (blue curve) and masses corresponding to united-atom representation (red curve). (For interpretation of the references to color in this figure legend, the reader is referred to the web version of this article.)

The ordering effect was also observed for cholesterol-enriched DPPC bilayers [47]. However, the mechanisms behind these effects are different. As shown in [47], cholesterol stays anchored at the level of the carbonyl groups of DPPC lipids thus ordering the

**Table 1**

Comparison of parameters of 9% DPPI bilayer calculated from the united-atom and from the coarse-grained simulations.

Parameter	United-atom	Coarse-grained
Area per lipid (nm <sup>2</sup> )	0.53	0.6
Volume per lipid (nm <sup>3</sup> )	1.14	1.15
Bilayer thickness (nm)	4.5	4.2
Lateral diffusion coefficient (10 <sup>-7</sup> cm <sup>2</sup> /s)	1.02	2.62

hydrocarbon chains via its rigid ring system. Altering the amount of cholesterol is a way to adopt the physical properties of the bilayer such as rigidity, water permeability and fluidity to the environment. In contrast to the ring system of cholesterol, large headgroups of PIP<sub>2</sub> extend into an aqueous phase above the level of choline groups. The DPPC lipids that are in direct contact with PIP<sub>2</sub> adopt their headgroup conformation nearly normal to the bilayer while in the pure DPPC membrane headgroups lie nearly parallel to the bilayer [22]. The AFM-type simulations demonstrated that pulling a DPPC lipid that is in direct contact with PIP<sub>2</sub> requires ~50% more work than pulling a DPPC lipid out of a pure DPPC bilayer. Thus PIP<sub>2</sub> forms a tight complex with the surrounding lipids which provides it with a resistance to a vertical displacement by anchoring proteins.

A different mechanism of choline groups reorientation and membrane compression was described for POPC/POPS bilayers suspended in 1 M salt solution [48]. Using the fluorescence solvent relaxation technique and molecular dynamics simulations performed in GROMACS the authors demonstrated that these changes are the consequences of adsorption of cations by the carbonyl groups of lipids. Presence of a cation-enriched part in the membrane causes rising of POPC headgroups while negatively charged POPS headgroups lie roughly parallel to the surface. Another effect of cations is bridging between neighboring lipid molecules that was reported previously from both simulations [49] and experiments [50]. However, simulations performed with the CHARMM force field revealed a preferred binding of Na<sup>+</sup> to the phosphate groups compared to the lipid ester carbonyl groups [51]. This contradiction between two force fields can be attributed to differences in vdW parameters of the ions or in the partial charges of the lipids headgroups. More comparative force field studies and experimental data are needed to establish which parameters reproduce ion-lipid interactions better. Nevertheless, it was concluded that a sodium cation can bind up to four lipids thus hindering their mobility. The number of Na-mediated clusters and their stability depend on the bilayer composition. As reported in the study of mixed acidic/zwitterionic bilayers, DMPS shows a stronger tendency to cluster around Na<sup>+</sup> and exclude neutral zwitterionic DMPC compared to other negatively charged lipids such as DMPG and DMPA [51]. On the one hand, this is due to the strong Na<sup>+</sup> binding affinity of the carboxylate group. On the other hand, the carboxylate group of DMPS is more likely to form an intermolecular hydrogen bond with the ammonium group of DMPS than with the choline group of DMPC. Thus DMPS lipids form a strong hydrogen-bond network in a DMPC bilayer. As a result DMPC/DMPS bilayer has a lower area per lipid and higher order parameters than pure DMPC and DMPS/DMPG bilayers. This is in agreement with the data indicating that PS lipids build rafts that play a role in the regulation of the cell cycle [52]. As mentioned earlier, PIP<sub>2</sub> is also known to locally increase its concentration but this process is presumably driven by proteins [11]. As described in [11], several natively unfolded proteins contain regions of basic/hydrophobic residues that bind to lipid membranes and sequester PIP<sub>2</sub> electrostatically. When the local intracellular Ca<sup>2+</sup> level increases, Ca<sup>2+</sup>/calmodulin binds to the basic region with high affinity and pulls it off the membrane, releasing PIP<sub>2</sub> and allowing it to perform its functions.

In conclusion we may say that the investigation of membrane-protein interactions requires simulations of larger membrane patches on timescales of hundreds of nanoseconds. To carry out such simulations the coarse-grained simulation methods are necessary. Our coarse-grained model of DPPC/DPPI lipid bilayer (Fig. 1B) reproduces main bilayer properties with 2.5-fold speed-up of dynamics. The DPPC/DPPI coarse-grained bilayer created in this study will be used for further investigation of membrane-protein interactions.

## Acknowledgments

This work was partially supported by RSF grant (#14-14-00234) to O.S.

## References

- [1] M. Marsh, H.T. McMahon, The Structural Era of Endocytosis, *Science* 285 (1999) 215–220 (80).
- [2] T. Lecuit, F. Pilot, Developmental control of cell morphogenesis: a focus on membrane growth, *Nat. Cell Biol.* 5 (2003) 103–108.
- [3] H.T. McMahon, J.L. Gallop, Membrane curvature and mechanisms of dynamic cell membrane remodelling, *Nature* 438 (2005) 590–596.
- [4] J. Zimmerberg, M.M. Kozlov, How proteins produce cellular membrane curvature, *Nat. Rev. Mol. Cell Biol.* 7 (2006) 9–19.
- [5] W. Cho, R.V. Stahelin, Membrane-protein interactions in cell signaling and membrane trafficking, *Annu. Rev. Biophys. Biomol. Struct.* 34 (2005) 119–151.
- [6] T. Itoh, K.S. Erdmann, A. Roux, B. Habermann, H. Werner, P. De Camilli, Dynamin and the actin cytoskeleton cooperatively regulate plasma membrane invagination by BAR and F-BAR proteins, *Dev. Cell* 9 (2005) 791–804.
- [7] K. Tsujita, S. Suetsugu, N. Sasaki, M. Furutani, T. Oikawa, T. Takenawa, Coordination between the actin cytoskeleton and membrane deformation by a novel membrane tubulation domain of PCH proteins is involved in endocytosis, *J. Cell Biol.* 172 (2006) 269–279.
- [8] P.K. Mattila, A. Pykäläinen, J. Saarikangas, V.O. Paavilainen, H. Vihinen, E. Jokitalo, et al., Missing-in-metastasis and IRSp53 deform PI(4,5)P<sub>2</sub>-rich membranes by an inverse BAR domain-like mechanism, *J. Cell Biol.* 176 (2007) 953–964.
- [9] A.N. Becalska, C.F. Kelley, C. Berciu, T.B. Stanishneva-Konovalova, X. Fu, S. Wang, et al., Formation of membrane ridges and scallops by the F-BAR protein Nervous Wreck, *Mol. Biol. Cell* 24 (2013) 2406–2418.
- [10] M. a Lemmon, K.M. Ferguson, Signal-dependent membrane targeting by pleckstrin homology (PH) domains, *Biochem. J.* 350 Pt 1 (2000) 1–18.
- [11] S. McLaughlin, D. Murray, Plasma membrane phosphoinositide organization by protein electrostatics, *Nature* 438 (2005) 605–611.
- [12] A. Hermelink, G. Brezesinski, Do unsaturated phosphoinositides mix with ordered phosphatidylcholine model membranes?, *J. Lipid Res.* 49 (2008) 1918–1925.
- [13] T.E. Rusten, H. Stenmark, Analyzing phosphoinositides and their interacting proteins, *Nat. Methods* 3 (2006) 251–258.
- [14] R. Kapeller, L.C. Cantley, Phosphatidylinositol 3-kinase, *BioEssays* 16 (1994) 565–576.
- [15] M.P. Czech, PIP<sub>2</sub> and PIP<sub>3</sub>: complex roles at the cell surface, *Cell* 100 (2000) 603–606.
- [16] T. Tanaka, D. Iwawaki, M. Sakamoto, Y. Takai, J. Morishige, K. Murakami, et al., Mechanisms of accumulation of arachidonate in phosphatidylinositol in yellowtail. A comparative study of acylation systems of phospholipids in rat and the fish species *Seriola quinqueradiata*, *Eur. J. Biochem.* 270 (2003) 1466–1473.
- [17] I. Liepina, C. Czaplowski, P. Janmey, A. Liwo, Molecular dynamics study of a gelsolin-derived peptide binding to a lipid bilayer containing phosphatidylinositol 4,5-bisphosphate, *Biopolymers* 71 (2003) 49–70.
- [18] S. Haider, A.I. Tarasov, T.J. Craig, M.S.P. Sansom, F.M. Ashcroft, Identification of the PIP<sub>2</sub>-binding site on Kir6.2 by molecular modelling and functional analysis, *EMBO J.* 26 (2007) 3749–3759.
- [19] E. Psachoulia, M.S.P. Sansom, Interactions of the pleckstrin homology domain with phosphatidylinositol phosphate and membranes: characterization via molecular dynamics simulations, *Biochemistry* 47 (2008) 4211–4220.
- [20] S. Brauchi, G. Orta, C. Mascayano, M. Salazar, N. Raddatz, H. Urbina, et al., Dissection of the components for PIP<sub>2</sub> activation and thermosensation in TRP channels, *Proc. Natl. Acad. Sci. USA* 104 (2007) 10246–10251.
- [21] P.D. Blood, R.D. Swenson, G. a Voth, Factors influencing local membrane curvature induction by N-BAR domains as revealed by molecular dynamics simulations, *Biophys. J.* 95 (2008) 1866–1876.
- [22] D. Lupyán, M. Mezei, D.E. Logothetis, R. Osman, A molecular dynamics investigation of lipid bilayer perturbation by PIP<sub>2</sub>, *Biophys. J.* 98 (2010) 240–247.
- [23] S.J. Marrink, H.J. Risselada, S. Yefimov, D.P. Tieleman, A.H. de Vries, The MARTINI force field: coarse grained model for biomolecular simulations, *J. Phys. Chem. B.* 111 (2007) 7812–7824.
- [24] S. Pronk, S. Páll, R. Schulz, P. Larsson, P. Bjelkmar, R. Apostolov, et al., GROMACS 4.5: a high-throughput and highly parallel open source molecular simulation toolkit, *Bioinformatics* 29 (2013) 845–854.
- [25] D.A. Holdbrook, Y.M. Leung, T.J. Piggot, P. Marius, P.T.F. Williamson, S. Khalid, Stability and membrane orientation of the fukutin transmembrane domain: a combined multiscale molecular dynamics and circular dichroism study, *Biochemistry* 49 (2010) 10796–10802.
- [26] A. Kukol, Lipid models for united-atom molecular dynamics simulations of proteins, *J. Chem. Theory Comput.* 5 (2009) 615–626.
- [27] I. Chandrasekhar, M. Kastenholtz, R.D. Lins, C. Oostenbrink, L.D. Schuler, D.P. Tieleman, et al., A consistent potential energy parameter set for lipids: dipalmitoylphosphatidylcholine as a benchmark of the GROMOS96 45A3 force field, *Eur. Biophys. J.* 32 (2003) 67–77.
- [28] T.J. Piggot, Á. Piñeiro, S. Khalid, Molecular dynamics simulations of phosphatidylcholine membranes: a comparative force field study, *J. Chem. Theory Comput.* 8 (2012) 4593–4609.
- [29] U. Essmann, L. Perera, M.L. Berkowitz, T. Darden, H. Lee, L.G. Pedersen, A smooth particle mesh Ewald method 103 (1995) 31–34.
- [30] M. Parrinello, A. Rahman, Polymorphic transitions in single crystals: a new molecular dynamics method, *J. Appl. Phys.* 52 (1981) 7182–7190.
- [31] S. Nose, M.L. Klein, Constant pressure molecular dynamics for molecular systems, *Mol. Phys.* 50 (1983) 1055–1076.
- [32] S. Nose, A molecular dynamics method for simulations in the canonical ensemble, *Mol. Phys.* 52 (1984) 255–268.
- [33] W.G. Hoover, Canonical dynamics: equilibrium phase-space distribution, *Phys. Rev. A* 31 (1985) 1695–1697.
- [34] S.J. Marrink, A.H. de Vries, A.E. Mark, Coarse grained model for semiquantitative lipid simulations, *J. Phys. Chem. B.* 108 (2004) 750–760.

- [35] C.A. López, A.J. Rzepiela, A.H. de Vries, L. Dijkhuizen, P.H. Hünenberger, et al., Martini coarse-grained force field: extension to carbohydrates, *J. Chem. Theory Comput.* (2009) 3195–3210.
- [36] O. V. Levtsova, I.D. Davletov, O.S. Sokolova, K. V. Shaitan, A molecular dynamics study of the interaction between domain I-BAR of the IRSp53 protein and negatively charged membranes, *Biophysics (Oxf)*. 56 (2011) 220–224.
- [37] S.O. Yesylevskyy, L.V. Schäfer, D. Sengupta, S.J. Marrink, Polarizable water model for the coarse-grained MARTINI force field, *PLoS Comput. Biol.* 6 (2010) e1000810.
- [38] V. Sadovnichy, A. Tikhonravov, V. Opanasenko, V. Voevodin, “Lomonosov”: Supercomputing at Moscow State University, in: J.S. Vetter (Ed.), *Contemp. High Perform. Comput. From Petascale Toward Exascale*, CRC Press, Boca Raton, USA, 2013, pp. 283–307.
- [39] N. Kucerka, J.F. Nagle, J.N. Sachs, S.E. Feller, J. Pencer, A. Jackson, et al., Lipid bilayer structure determined by the simultaneous analysis of neutron and X-ray scattering data, *Biophys. J.* 95 (2008) 2356–2367.
- [40] N. Kučerka, M.-P. Nieh, J. Katsaras, Fluid phase lipid areas and bilayer thicknesses of commonly used phosphatidylcholines as a function of temperature, *Biochim. Biophys. Acta* 2011 (1808) 2761–2771.
- [41] H.I. Petrache, S.W. Dodd, M.F. Brown, Phosphatidylcholines determined by <sup>2</sup>H NMR spectroscopy 79 (2000) 3172–3192.
- [42] J.F. Nagle, S. Tristram-Nagle, Structure of lipid bilayers, *Biochim. Biophys. Acta – Rev. Biomembr.* 1469 (2000) 159–195.
- [43] N. Kucerka, S. Tristram-Nagle, J.F. Nagle, Closer look at structure of fully hydrated fluid phase DPPC bilayers, *Biophys. J.* 90 (2006) L83–L85.
- [44] J.P. Douliez, A. Léonard, E.J. Dufourc, Restatement of order parameters in biomembranes: calculation of C–C bond order parameters from C–D quadrupolar splittings, *Biophys. J.* 68 (1995) 1727–1739.
- [45] J.R. Sheats, H.M. McConnell, A photochemical technique for measuring lateral diffusion of spin-labeled phospholipids in membranes, *Proc. Natl. Acad. Sci. USA* 75 (1978) 4661–4663.
- [46] D. Van Der Spoel, E. Lindahl, B. Hess, G. Groenhof, A.E. Mark, H.J.C. Berendsen, GROMACS: fast, flexible, and free, *J. Comput. Chem.* 26 (2005) 1701–1718.
- [47] C. Hofsäss, E. Lindahl, O. Edholm, Molecular dynamics simulations of phospholipid bilayers with cholesterol, *Biophys. J.* 84 (2003) 2192–2206.
- [48] P. Jurkiewicz, L. Cwiklik, A. Vojtíšková, P. Jungwirth, M. Hof, Structure, dynamics, and hydration of POPC/POPS bilayers suspended in NaCl, KCl, and CsCl solutions, *Biochim. Biophys. Acta* 2012 (1818) 609–616.
- [49] A.A. Gurtovenko, Asymmetry of lipid bilayers induced by monovalent salt: atomistic molecular-dynamics study, *J. Chem. Phys.* 122 (2005) 244902.
- [50] E. Leontidis, A. Aroti, Liquid expanded monolayers of lipids as model systems to understand the anionic hofmeister series: 2. Ion partitioning is mostly a matter of size, *J. Phys. Chem. B* 113 (2009) 1460–1467.
- [51] T. Broemstrup, N. Reuter, Molecular dynamics simulations of mixed acidic/zwitterionic phospholipid bilayers, *Biophys. J.* 99 (2010) 825–833.
- [52] C. Kantari, M. Pederzoli-Ribeil, O. Amir-Moazami, V. Gausson-Dorey, I.C. Moura, M.-C. Lecomte, et al., Proteinase 3, the Wegener autoantigen, is externalized during neutrophil apoptosis: evidence for a functional association with phospholipid scramblase 1 and interference with macrophage phagocytosis, *Blood* 110 (2007) 4086–4095.